Title

Test of Scintillometer Saturation Correction Methods Using Field Experimental Data

Journal

Boundary-Layer Meteorology, 137(3)

ISSN

0006-8314 1573-1472

Authors

Kleissl, J.
Hartogensis, O. K
Gomez, J. D

Publication Date

2010-10-06

DOI

10.1007/s10546-010-9540-x

Peer reviewed

Boundary Layer Meteorology manuscript No.
(will be inserted by the editor)

Test of scintillometer saturation correction methods using field experimental data

J. Kleissl, O.K. Hartogensis, J.D. Gomez

Received: Aug. 11, 2009 / Accepted: date

Abstract Saturation of large aperture scintillometer (LAS) signals can result in sensible heat flux measurements that are biased low. A field study with LASs of different aperture sizes and path lengths was performed to investigate the onset of and corrections for signal saturation. Saturation already occurs at $C_n^2 \approx 0.074 D^{5/3} \lambda^{1/3} L^{-8/3}$, where C_n^2 is the structure parameter of the refractive index, D is the aperture size, λ is the wavelength, L is the transect length, which is smaller than theoretically derived saturation limits. At a transect length of 1 km, a height of 2.5 m, and aperture ≈ 0.15 m the correction factor exceeds 5% already at $C_n^2 = 2 \times 10^{-12}$ m$^{-2/3}$, which will affect many practical applications of scintillometry.

The Clifford correction method, which only depends on C_n^2 and transect geometry, provides good saturation corrections over the range of conditions observed in our study. The saturation correction proposed by Ochs and Hill results in correction factors that are too small in large saturation regimes. An inner length scale dependence of the saturation correction factor was not observed. Thus for practical applications the Clifford correction method should be applied.

Keywords Large aperture scintillometer · Sensible heat flux · Signal saturation · Wave propagation

1 Introduction

A major challenge for the validation of surface energy balance fluxes from remote sensing images is the ground measurement at a scale similar to their spatial resolution. While the pixel size of daily thermal remote sensing images is on the order of km,

J. Kleissl
Dept. of Mechanical and Aerospace Engineering, University of California, San Diego, USA
Tel.: +1-443-527-2740
E-mail: jkleissl@ucsd.edu

J.D. Gomez
Dept. of Earth and Environmental Sciences, New Mexico Tech, Socorro, New Mexico, USA

O.K. Hartogensis
Dept of Meteorology and Air Quality, Wageningen University, Wageningen, The Netherlands

existing methods to measure sensible heat fluxes have a footprint at a considerably smaller scale. Large aperture scintillometers (LAS) offer the unique possibility of measuring the vertical flux of sensible heat H averaged over areas comparable to one or more pixels of a satellite image or mesoscale numerical weather model (Andreas 1990; Hill et al. 1992; Meijninger et al. 2002; Hemakumara et al. 2003; Hafeez et al. 2006; Hartogensis and De Bruin 2005; Ezzahar et al. 2007; Hendrickx et al. 2007; Kleissl et al. 2009b).

A LAS receiver measures intensity I fluctuations in the radiation emitted by the transmitter at a distance of 500 - 10,000 m to derive the structure parameter of the refractive index, C_n^2 [$\mathrm{m}^{-2/3}$]. Refractive scattering by density variations due to turbulent eddies along the propagation path causes these intensity fluctuations. The LAS beam height and set-up distance have to be chosen, such that it operates in the weak scattering regime, where C_n^2 is small enough that it can be derived from the variance of the natural log of signal intensity $\sigma_{\ln I}^2$ from first-order scattering theory (Wang et al. 1978) as

$$\sigma_{\ln I}^2 = 0.89 C_n^2 D^{-7/3} L^3, \tag{1}$$

where D is the aperture diameter and L is the transect length. Eq. 1 is only valid as long as $\sigma_{\ln I}^2$ does not exceed a certain threshold. $\sigma_{\ln I}^2$ decreases with D since it leads to filtering of the effect of the predominant small scale inhomogeneities, and increases with L, since longer path lengths imply that the light encounters more distorting irregularities which invalidate the first-order scattering theory (see also Clifford et al., 1974, hereinafter C74). For the optical scintillometers at hand, C_n^2 is mainly dependent on the surface sensible heat flux but also decreases with height above the land surface z_{eff} (Hartogensis and de Bruin 2005; in free convective conditions C_n^2 is proportional to $(z_{\mathrm{eff}}/L_o)^{-4/3}$, where L_o is the Obukhov length).

Thus, to avoid saturation and ensure the validity of Eq. 1, D, L and C_n^2 are bounded to certain limits. Saturation-free operation of a scintillometer can be achieved by increasing the aperture. For a laser scintillometer D should be replaced by $\sqrt{\lambda L} \approx 10$ mm (λ is the wavelength) and saturation occurs already at distances of about 200 m. To extend the application of scintillometers to longer pathlengths Wang et al (1978) developed the theory for a Large Aperture Scintillometer, which was introduced as an inner-scale independent and saturation resistant scintillometer. However, also the LAS is bounded to limits in L and C_n^2.

For weak scattering, C_n^2 and $\sigma_{\ln I}^2$ are linearly related as per Eq. 1. For "strong weak" scattering, saturation means that an increase in C_n^2 causes an increase in $\sigma_{\ln I}^2$ which is smaller than the linear increase predicted by Eq. 1. Consequently, a (small) correction has to be applied. For *strong* scattering (large H, small D, or large L), $\sigma_{\ln I}^2$ no longer increases, i.e. the signal intensity variation is 'saturated' and Eq. 1 no longer holds resulting in an underestimation of H which cannot be corrected. Since D is an instrument constant and the maximum expected H is an environmental parameter specific to the site, the longer the path L the higher the LAS needs to be installed to avoid saturation (Hartogensis et al., 2003). Consequently, large installation heights are often required in arid regions. Improved knowledge about the onset of saturation and saturation corrections can mitigate the cost and maintenance issues associated with increasing z_{eff} e.g. through the use of towers.

Kohsiek et al. (2006) compared H from an extra large aperture scintillometer (XLAS) over a pathlength of 10 km to eddy covariance (EC) estimates. Applying

a correction based on Frehlich and Ochs (1990) resulted in overestimation of H, while the Hill and Clifford (1981) correction matched the eddy covariance estimates. We extend the analysis of Kohsiek et al. (2006) by employing an experimental set-up that allows comparing C_n^2 with variations in path length and aperture diameter (Kleissl et al. 2008b). Note that the log-variance of the signals in our experiment are so large that deviations up to about 45% from the LAS formula (Eq. 1) occur which are pushing the limit of the weak scattering regime. We acknowledge that our eddy covariance data were not suitable to evaluate C_n^2 from the temperature spectra, so unlike Kohsiek et al. (2006) we compared C_n^2 from scintillometers at different saturation levels.

The overall objective is to determine a validated expression for the onset of saturation, and to test empirical correction procedures using a saturation correction factor m which is the ratio of the real C_n^2 divided by the observed C_n^2. Sections 2, 3, 4, and 5 describe the theory, field experiment and data processing, results, and conclusions, respectively.

2 Saturation Theory and Corrections

To avoid repetition, we provide only a brief review of saturation here and refer to Moene et al. (2004) and Kohsiek et al. (2006) for further details. Most scintillometer theory relies on the assumption of isotropic and homogeneous turbulence which is expected to be true given the small scales affecting the measurements. In strong turbulence an increase in C_n^2 causes $\sigma_{\ln I}$ to increase by less than dictated by Eq. 1 or not at all. This saturation can be conceptualized to occur with the breakdown of the single scattering theory in that an already distorted wave front is focused by another inhomogeneity onto the receiver lense resulting in additional "smearing" of the wavefront but not a change in signal intensity variation. The effect of increasing saturation is that the scintillometer becomes increasingly sensitive to fluctuations at small scales (increasingly smaller than the beam diameter).

The theoretical framework of scintillometer saturation is based on Hill (1981)

$$\sigma_{\ln I}^2 = 16\pi^2 k^2 L \int_0^1 du \int_0^\infty d\kappa\kappa\Phi_n(\kappa)\sin^2\left[\frac{\kappa L u(1-u)}{2k}\right]\left[\frac{2J_1(x_1)}{x_1}\frac{2J_1(x_2)}{x_2}\right]^2 M_{\mathrm{ST}}, \tag{2}$$

where k is the optical wavenumber, κ is the spatial wavenumber, $\Phi_n(\kappa) = 0.033 C_n^2 \kappa^{-11/3} f(\kappa l_o)$, $x_1 = \kappa D u/2$, $x_2 = \kappa D(1-u)/2$, J_1 is the Bessel function of the first kind and first order, and u is the normalized path position. C74 and Hill (1981) accounted for saturation through the modulation transfer function M_{ST} which in Hill (1981) is defined as

$$M_{\mathrm{ST}} = \exp\left\{-48k^2 L\left[\kappa\Psi(\kappa)\left(1 - J_o(\kappa^2 U)\right) + \int_\kappa^\infty d\kappa'\Psi(\kappa')\left(1 - J_o(\kappa'\kappa U)\right)\right]\right\}, \tag{3}$$

where $U = Lu(1-u)/k$, $\Psi(\kappa) = \int_\kappa^\infty \Phi_n(\kappa')d\kappa'$, and J_o is the Bessel function of the first kind and zeroth order . If $f(\kappa l_o) = 1$ as in C74, then Eq. 3 is independent of the inner length scale. The C74 correction is one of the corrections applied in this paper.

From Eq. 2, C74 found that Eq. 1 becomes modified by an exponential term involving $\sigma_{\ln I,o}^2$, where the subscript "o" indicates that term is derived from first order theory.

C74 state that the exponential term becomes small for $\sigma^2_{\ln I,o} < 0.3$, but for a spherical wave from a point source Moene et al. (2004) showed that Clifford's expression still results in a saturation correction of 15% for $\sigma^2_{\ln I} = 0.3$.

Hill (1981) found the inner length scale l_o to be a relevant parameter for saturation corrections. Hill's (1981) correction (his Eq. 5) is derived for weak scattering and includes inner scale effects that – independent of saturation – are expected to occur when $D/l_o < 20$ (Hill and Ochs, 1978; Moene et al., 2005; Hartogensis, 2006). Considering that "strong weak" scattering occurs in our experiment, and that $D = 0.15$ m, inner scale effects are expected for l_o even less than 7.5 mm.

The introduction of the Hill bump for $f(\kappa l_o)$ expands the C74 theory to correct for both saturation and l_o effects. To describe the Hill bump in $f(\kappa l_o)$, Kohsiek et al. (2006) used the analytic approximation of Frehlich (1992) and developed a similar one for $\Psi(\kappa)$. The MATHCAD algorithm employed in this paper, developed by Meijninger (personal communication, 2006), also uses the Frehlich (1992) approximation for $f(\kappa l_o)$, whereas $\Psi(\kappa)$ is evaluated numerically. This correction termed OH82 after Ochs and Hill (1982) is also applied in this paper.

For LASs with equal aperture diameters of receiver and transmitter, most criteria for the *onset* of significant saturation are based on an expression of type

$$D/\left(\lambda L\right)^{1/2} > A\left(0.124k^{7/6}L^{11/6}C_n^2\right)^B, \tag{4}$$

where the left hand side is a non-dimensional ratio of aperture diameter and Fresnel zone λL while the right hand side takes into account the transect length, C_n^2, and constants A and B. Often it is more useful to solve Eq. 4 for C_n^2 to confirm operation in saturation free conditions. Wang et al. (1978) found $A = 0.98, B = 3/5$; from theoretical arguments OH82 found saturation to occur already for $A = 2.7, B = 3/5$; Frehlich and Ochs (1990) found $A = 5.4$ and $B = 3/5$; finally Moene et al. (2004) examined the validity of the first-order scattering approximation using the full equation for wave propagation including strong scattering ($A = 1.6$, $B = 1/2$ and the left hand side of Eq. 4 must be much greater than the right hand side).

3 Field Experiment and Data Processing

This section describes the experimental setup (section 3.1) and the processing of eddy covariance data (section 3.2). Due to differences in the scintillometer instrument gain, a cross calibration was applied in post-processing (section 3.3). Saturation corrections are described in section 3.4.

3.1 Field site and set-up

An experiment, specifically designed to study saturation, was conducted from July 11 to August 24, 2007 (Table 1, Figs. 1, 2). Two LASs, one XLAS (all Kipp & Zonen, The Netherlands), a BLS900 (Scintec, Germany), and an eddy covariance station were set-up over arid grassland at a height of ≈ 2.5 m in the Sevilleta National Wildlife Refuge (near 348262 m northing, 3806021 m easting, 1590 m above mean sea level, UTM12), 70 km south of Albuquerque, New Mexico, USA. Daily afternoon cumulus

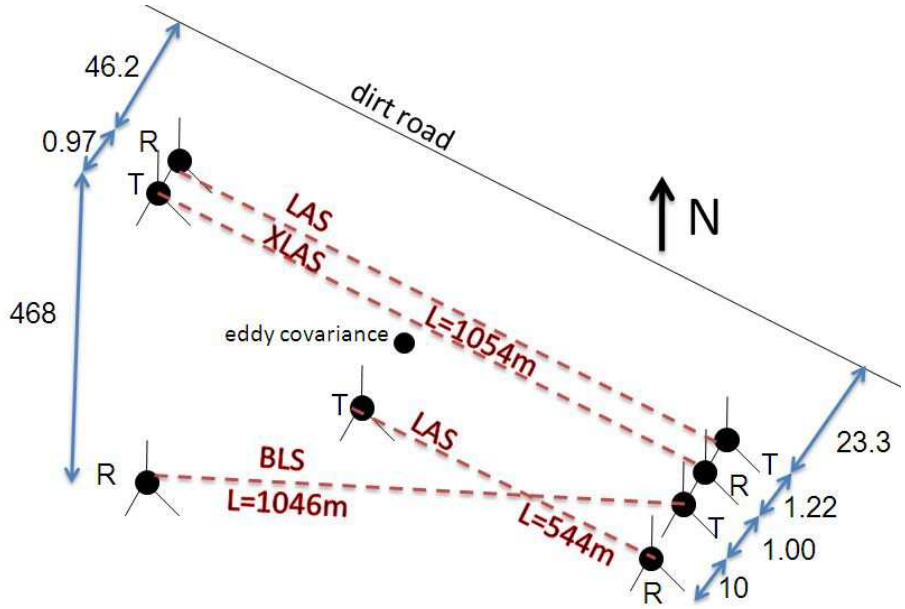

Fig. 1 Bird's eye view of the set-up. All distances are in metres. "R" marks receiver, and "T" marks transmitter locations.

clouds and intermittent rainfall occurred during the Monsoon season with a total rainfall of 14.3 mm occurring on 8 days. Typical meteorological conditions at noon were $R_{net} = 550$ W m^{-2}, Bowen ratio of one, and 2.5 m wind speeds of 2-6 m s^{-1}.

One LAS (LASL1050m), the BLS900, and the XLAS were set-up with a path length of $L \approx 1050$ m; the other LAS (LASL544m) covered a path length of $L = 544$ m. Using Eq. 4 with the OH82 parameters we estimate that for the LASL1050m $C_n^2 > 6.2 \times 10^{-13}$ m$^{-2/3}$ (corresponding to a sensible heat flux of 203 W m^{-2} in free convective conditions) would result in saturation (Table 1). Since the aperture diameter D of the XLAS is more than twice that of the LAS, it is sensitive to larger turbulence scales resulting in weaker measured scintillations making it more saturation resistant. Consequently, with our set-up the effect of sensible heat flux, D, and L on saturation could be determined and appropriate correction models tested. Based on Eq. 4, doubling D (XLAS) is expected to delay the onset of saturation, but not by as much as halfing L (LASL544m).

The LASs and XLAS analog output of C_n^2 and signal strength voltage were sampled at 1 Hz and stored as 1-min averages on a CR10X and a CR1000 datalogger (both Campbell Scientific Inc.), respectively. The C_n^2 computed internally was corrected for the difference between geometric and effective aperture diameter (Kleissl et al. 2008a).

The BLS900 collimates 2 transmitter beams by plane convex lenses onto two Si photodiodes. Absorption fluctuations may be falsely interpreted as scintillations, hence artificially increasing the derived H. Using the "two-in-one" configuration of the BLS900, C_n^2 could be corrected for absorption fluctuations due to dust or humidity. To standardize the intercomparison, the two beams in the BLS900 were treated as two separate transects and the absorption correction was not applied. The saturation correction and extinction and outer scale corrections as suggested by the Scintec processing software

Fig. 2 Photograph of the south-east set-up with (from left to right) LASL1050m transmitter, XLAS receiver, BLS900 transmitter. The receiver of LASL544m is 10 m to the right.

were also not applied [for other applications we recommend using these features to obtain a more accurate C_n^2 (Kleissl et al. 2008b)]. The BLS900 has an internal signal processing and digital data storage unit. The BLS900 transmitter was set to a pulse frequency of 5 Hz and averages and variances of the signal strength were calculated over 1-min intervals.

Special care was taken to accurately determine the relative height of the transmitters and receivers using laser level measurements resulting in accuracies of ≈ 0.025 m or 1% of the beam height. Waypoints were taken about every 10 m underneath the transects with a Differential Global Positioning System (DGPS, absolute vertical accuracy ≈ 0.1 m) to establish the transect profile and the beam height (Fig. 3). Although the heights above ground level (a.g.l.) of each instrument were nearly identical, uneven terrain caused the effective transect heights to range from 2.50 to 2.90 m. Errors in the transect length were less than 2 m and can be neglected (Hartogensis et al. 2003).

An eddy-covariance (EC) energy balance tower near the center of the transects (Fig. 1) was instrumented at 2.51 m a.g.l. with a Licor Li7500 open path CO_2/H_2O infrared gas analyzer (IRGA) and a Campbell Scientific 3D sonic anemometer-thermometer (CSAT3) both sampled and stored at 10 Hz. Furthermore, we deployed a Kipp and Zonen CNR1 four component radiometer, an Apogee IRR-P infrared thermometer, two soil heat flux probes with soil temperature and soil moisture sensors, and a tipping bucket rain gauge. All low-frequency measurements were sampled every second and stored as one minute averages. From the eddy covariance measurements, roughness

Table 1 Properties of the scintillometer transects. D: effective aperture diameter, L: transect length, z: average height of transmitter and receiver above ground level, z_{eff}: effective beam height, $C^{2,sat}_{n,\text{OH82}}$: onset of saturation according to Eq. 4 with the OH82 constants. All instruments use a wavelength of $\lambda = 880$ nm. The last 3 rows give the correlation coefficient ρ and calibration factors ($y = ax + b$) applied to C_n^2 from the scintillometers to make them the same as C_n^2 from XLAS in unstable conditions.

Scintillometer	BLS900	XLAS	LASL1050m	LASL544m
Serial number	T-E 0059	040002	030005	070045
D [m]	0.145	0.32	0.147	0.147
L [m]	1047	1049	1050	544
z [m]	2.52	2.51	2.51	2.74
z_{eff} [m]	2.90	2.59	2.59	2.50
Lense	convex glass	Fresnel		
Transmitter	multi-LED	single LED		
$C^{2,sat}_{\text{n,OH82}}$ [$\text{m}^{-2/3}$]	6.12×10^{-13}	2.28×10^{-12}	6.22×10^{-13}	3.59×10^{-12}
ρ	0.862	1	0.968	0.920
a [-]	0.656	1	0.870	0.521
b[10^{-15} $\text{m}^{-2/3}$]	-15.2	0	2.77	-5.47

length and zero displacement height were determined as $z_o = 0.047$ m and $d = 0.01$ m (Martano, 1999).

3.2 Eddy Covariance data processing

The eddy covariance data were processed with the latest version of the EC-pack software package (www.met.wau.nl/projects/jep), developed by Wageningen University. The following corrections were performed in calculating the 10-minute averaged fluxes:

- axis rotations around the x- and y-axes of the CSAT3 coordinate system with the planar fit routine (Wilczak et al. 2001). The planar fit rotation angles were determined for each day. The rotation into the mean horizontal wind, around the z-axis, was done for every flux interval;
- CSAT3 temperature correction for the influence of humidity on the speed of sound measurement (Schotanus et al., 1983);
- fluxes correction for poor frequency response (Moore, 1986).

Due to dropped samples by the datalogger the quality of the eddy covariance spectra was not good enough to determine C_n^2 and the dissipation rate of turbulence kinetic energy (TKE) from the inertial range of the vertical velocity w. Thus we only used the eddy covariance data to calculate l_o from the fluxes (which are less affected by uneven sampling) using

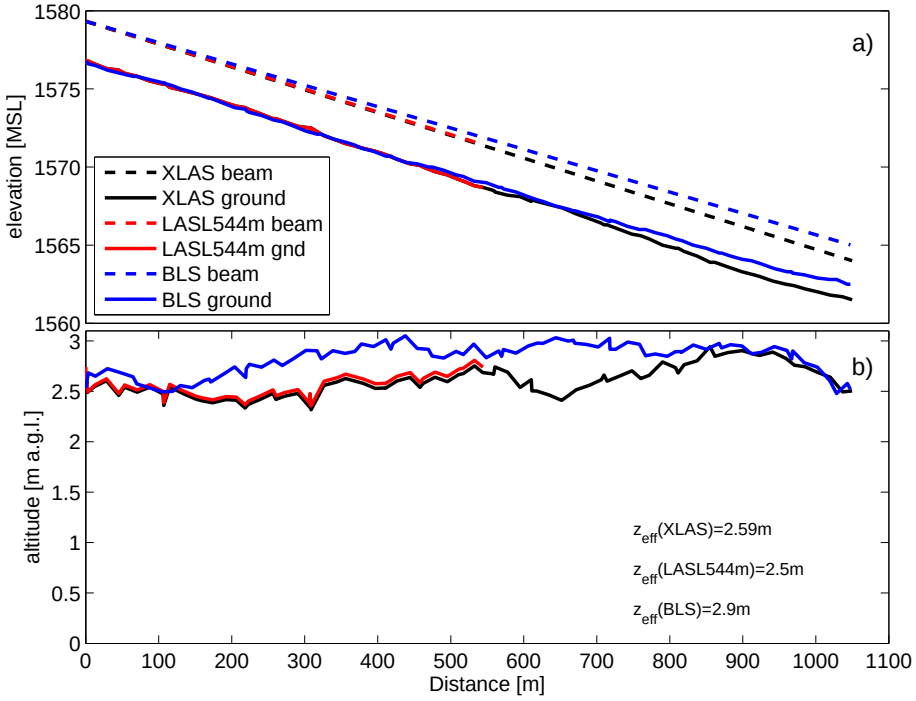

Fig. 3 Transect heights as measured by a DGPS. The high point is at the south-east end of the transect. a) Beam and ground elevation; b) Beam height. The LASL1050m transect is identical with the XLAS transect and is not shown separately. Effective beam heights for free convective conditions are given on the bottom right.

$$l_o = 7.4 \left(\frac{\nu}{u_*}\right)^{3/4} \left(\frac{\kappa z}{f_\epsilon(\zeta)}\right)^{1/4}, \tag{5}$$

which combines the relation between l_o and the dissipation rate of TKE, ϵ, $\left[l_o = 7.4(\epsilon/\nu^3)^{-1/4}\right]$ with the Monin-Obukhov Similarity Theory dimensionless group for ϵ. Further, ν is the kinematic viscosity of air, which is empirically related to T [^{o}C] and air density ρ [kg m^{-3}]: $\nu = [1.718 + 0.0049T/\rho] \times 10^{-5}$[m^2 s^{-1}] (Thiermann, 1996). The factor 7.4 is reviewed by Hill (1997) and reflects the values 0.43 for the Obukhov-Corrsin constant and 0.72 for the Prandtl number. For stability parameter $\zeta > 0$, $f_\epsilon = 0.8 + 2.5\zeta$ (Hartogensis and De Bruin, 2005) and for $\zeta < 0$, $f_\epsilon = (1 - 15.1\zeta)^{-1/3} - \zeta - 0.16$ (Frenzen and Vogel, 1992) were used.

3.3 Scintillometer cross-calibration

All output was reprocessed with the effective beam height (Table 1) to rescale the height-dependent C_n^2 to effective beam height of the LASL1050m and XLAS ($z_{\text{eff}} = 2.59$ m), using the free convection scaling of constant $z_{\text{eff}}(C_T^2)^{3/4}$. Kleissl et al. (2008a) and Hartogensis et al. (2008) found significant differences between heat fluxes measured

by different Kipp & Zonen LASs over identical transects. However, the correlation coefficients between the LASs were very large indicating a problem with the gain that could be corrected if the true C_n^2 was known. On the other hand, Kleissl et al. (2009a) observed that four Scintec BLSs only differed by 3% or less. While we would expect the BLS900 to measure the most accurate C_n^2, the XLAS was selected as a reference for the cross-calibration since it was resistant to saturation had the longest data record.

Cross-calibration is necessary to correct the measurement error stemming from different LAS and XLAS gains and ensure accurate determination of saturation limits. Assuming that saturation was absent for $C_n^2 < 3 \times 10^{-13}$ m$^{-2/3}$ (motivated by our results in section 4.3), a linear regression between the reference C_n^2, taken from LASL1050m, and the other scintillometers was applied (Table 1). The correlation coefficients (ρ) were very large between the LASL1050m and XLAS which were located only 1 m apart at identical L. The two LASs were also highly correlated, although their L differed. The displaced BLS transect was less correlated to LASL1050m. The regression slopes reconfirm the significant inconsistencies associated with Kipp & Zonen scintillometers observed by Kleissl et al. (2008a) and Hartogensis et al. (2008).

Note that all instruments used in this study were new or had been factory calibrated recently. The BLS900 was purchased in November 2006, the LASL544m was purchased in 2007, and the LASL1050m had been recalibrated in July 2006. So the need for recalibrating the K&Z scintillometers was not caused by poor preparation of the experiment, but by inconsistencies in the instrumentation stemming from the manufacturer. However, when these inconsistencies are removed by a linear regression they should not affect the ensuing saturation analysis.

3.4 Saturation corrections

In this section saturation correction factors $m = C_{n,\mathrm{ref}}^2 / C_n^2$ are defined that will be tested in section 4. C_n^2 is the (calibrated) value from the saturated $\sigma_{\ln I}^2$ measurement, and $C_{\mathrm{n,ref}}^2$ is the real C_n^2. Since the full saturation correction of OH82 requires complicated and time-consuming mathematical calculations, we follow Kohsiek et al. (2006) and apply a third order multivariate regression

$$m = \sum_{i=1}^{10} c_i \left(C_n^2\right)^{A_i} (l_o)^{B_i}, \tag{6}$$

where A_i, B_i, and c_i depend on aperture diameter and pathlength (Table 2).

For the C74 correction (that is independent of l_o; Eq. 3 with $f = 1$), $B_i = 0$ and c_i and A_i are given at the top of Table 2. Using a numerical look-up table, Scintec's BLSRun data processing software applies the C74 saturation correction operationally. Fig. 5 shows a graphical depiction of Eq. 6 and Table 2, i.e. the saturation correction factors are plotted against the measured C_n^2 for the four scintillometer set-ups. As expected, the saturation correction for the LASL1050m is largest. Even the XLAS saturates somewhat, while the LASL544m can be considered saturation free with less than a 5 % correction for $C_n^2 < 10^{-12}$ m$^{-2/3}$. OH82 and C74 corrections are qualitatively consistent, but OH82 is more linear than C74 and also depends on l_o. The C74 correction is generally greater than the OH82 correction, especially for larger C_n^2.

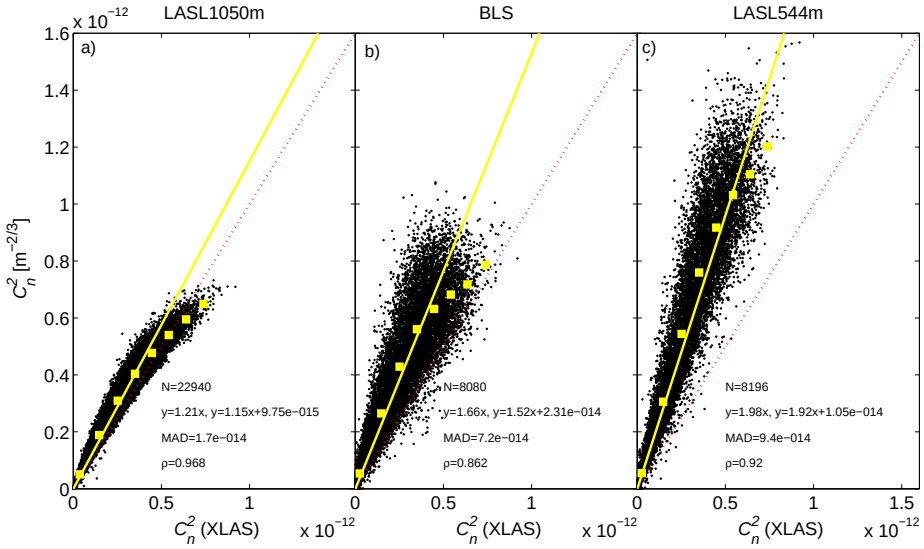

Fig. 4 Scatter plots of one minute averages of C_n^2 from XLAS (x-axis) versus the other scintillometers. For the BLS900 only beam 1 is shown. The text indicates statistical measures for the data for which $C_n^2 < 3 \times 10^{-13}$ m$^{-2/3}$, i.e. without saturation: the regression equations $C_n^2 = aC_{n,\mathrm{XLAS}}^2$ and $C_n^2 = aC_{n,\mathrm{XLAS}}^2 + b$, the mean absolute deviation mean$\left|C_{n,\mathrm{XLAS}}^2 - C_n^2\right|$, the correlation coefficient $\rho(C_{n,\mathrm{XLAS}}^2, C_n^2)$, and number of 1 min samples N. The red dotted line is the 1:1 line. The yellow solid line is the linear regression. The yellow squares are binned averages of C_n^2.

Table 2 Saturation correction equation coefficients based on Kohsiek et al. 2006 and Eq. 6. The coefficients are only valid for the setup for which they were computed.

			LASL1050m / BLS	XLAS	LASL544m
i	A_i	B_i	c_i for C74		
1	3	0	6.468×10^{34}	9.256×10^{33}	5.029×10^{32}
2	2	0	9.178×10^{22}	-5.574×10^{21}	2.062×10^{21}
3	1	0	2.972×10^{11}	1.324×10^{11}	5.464×10^{10}
4	0	0	1	0.998	1
i	A_i	B_i	c_i for OH82		
1	3	0	0	0	0
2	2	0	-2.467×10^{9}	-1.064×10^{8}	7.467×10^{7}
3	2	1	-1.798×10^{7}	-3.096×10^{6}	2.435×10^{5}
4	1	0	4.307×10^{11}	1.223×10^{11}	6.548×10^{10}
5	1	1	-3.593×10^{13}	-1.093×10^{13}	-5.991×10^{12}
6	1	2	1.068×10^{15}	3.435×10^{14}	1.855×10^{14}
7	0	0	1.009	1.011	1.012
8	0	1	-7.015	-8.801	-8.768
9	0	2	918.132	1.233×10^{3}	1.118×10^{3}
10	0	3	-3.016×10^{4}	-3.643×10^{4}	-3.631×10^{4}

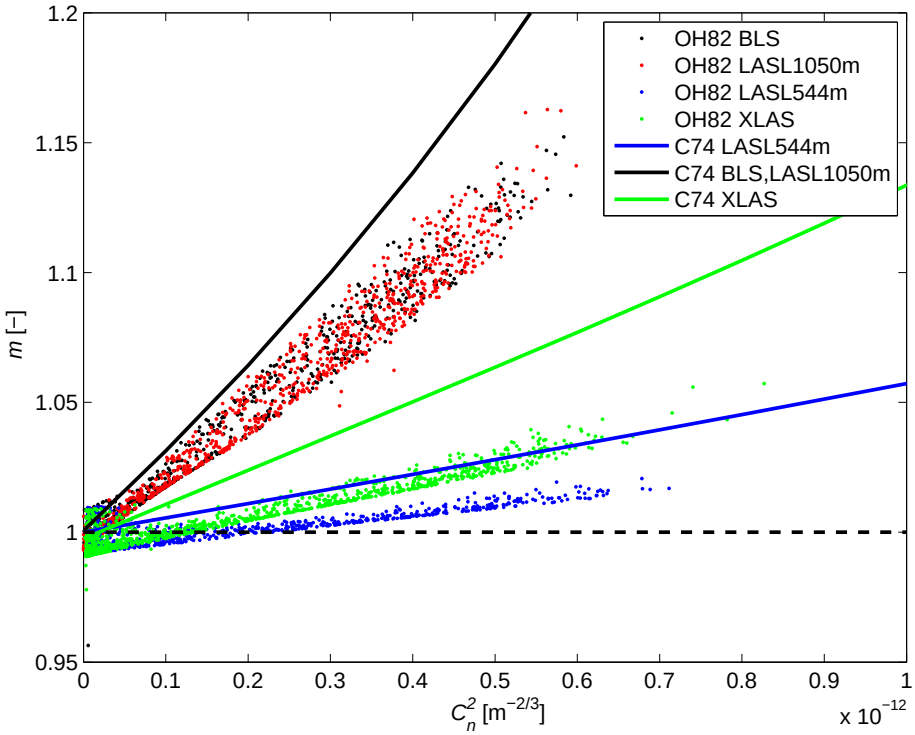

Fig. 5 Correction factor for saturation ($m = C^2_{n,\mathrm{ref}}/C^2_n$) as a function of measured C^2_n in OH82 (dots) and C74 (lines) for different path lengths and aperture sizes (Eq. 6, Table 2). The l_o dependence of OH82 is evident in the vertical range of the cloud of points which increases with m.

4 Results

4.1 Saturation and correction functions as function of C_n^2 only

Fig. 6 is similar to Fig. 4 but shows the C_n^2 corrected for instrument error using the calibration equations of Table 1. Figure 6 demonstrates the saturation limits of different scintillometers. Figure 6a, LASL1050m against XLAS, shows a decreasing ratio $C^2_{n,\mathrm{LAS}}/C^2_{n,\mathrm{XLAS}}$ for increasing C_n^2, an indicator of saturation of the LASL1050m. LASL544m (Fig. 6b) data are spread around the 1:1 line, indicating that the saturation over the short averaging path is similar to the saturation of the extra large aperture over the long path. The BLS saturates similarly as the LASL1050m with a stronger saturation for $C_n^2 > 0.6 \times 10^{-12}$ m$^{-2/3}$, but there is more spread in the data due to the larger distance between the transects (Fig. 1). Fig. 6 also shows the C74 and OH82 correction functions for C_n^2 (Table 2). In Fig. 6d for the LASL1050m, the C74 saturation correction falls within the inter-quartile range of the observed deviation due to saturation, while the OH82 saturation correction is too small. The strong saturation of the BLS900 for $C_n^2 > 0.6 \times 10^{-12}$ m$^{-2/3}$ is not predicted by either C74 or OH82. While theory predicts that the LASL544m would not saturate as much as the XLAS, for $C_n^2 > 0.6 \times 10^{-12}$ m$^{-2/3}$ the C_n^2 from LASL544m becomes significantly smaller than

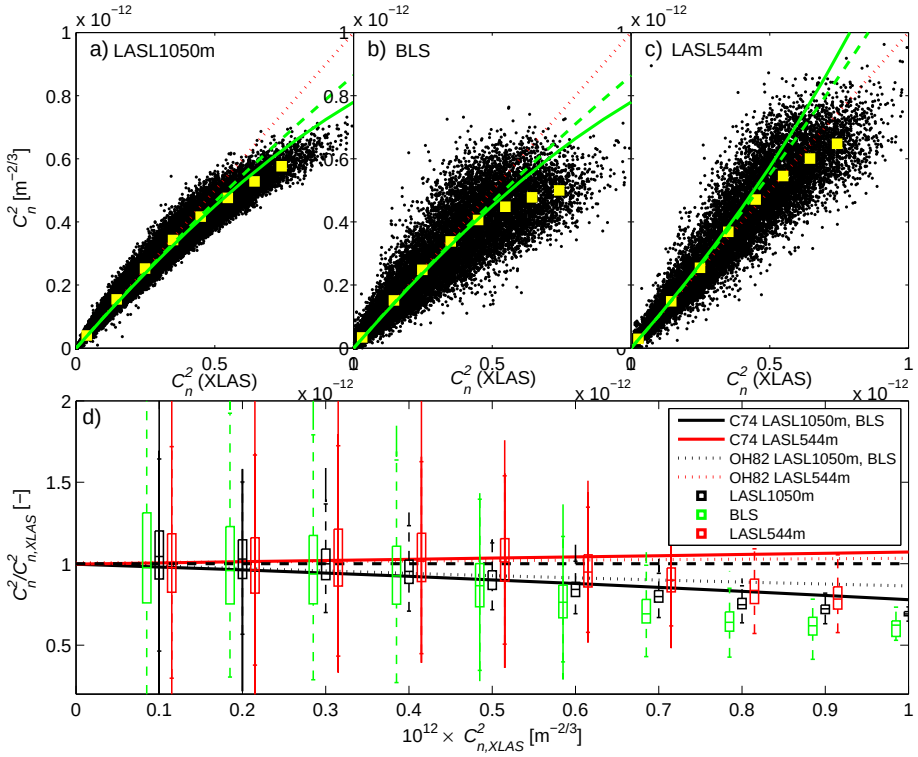

Fig. 6 a-c) Scatter plots of one minute averages of C_n^2 from XLAS (x-axis) versus the *calibrated* other scintillometers (black dots). The red dotted line is the 1:1 line representing the expected behaviour without saturation. The yellow squares are binned averages of C_n^2. The solid green lines shows the theoretically expected relationship between the C_n^2 of the two scintillometer based on C74, e.g. in a) it shows $m_{\mathrm{XLAS}}/m_{\mathrm{LASL1050m}}$ (Eq. 6). The dashed green line shows the OH82 correction where the inner scale was set to $l_o = 7.5$ mm in Eq. 6. d) Box and whisker plot of the ratio of C_n^2 from each scintillometer versus XLAS with horizontal lines at the lower quartile, median, and upper quartile values. The whiskers are lines extending from each end of the boxes to show the extent of the rest of the data. Lines show the ratios predicted by C74 and OH82.

the C_n^2 from the XLAS. A possible explanation is a change in the effective aperture size of LASL544m. A decrease in the LASL544m effective aperture would cause both the increase in saturation observed in Fig. 6b and the increase in measured C_n^2 in Fig. 4b. In the following we will only use the XLAS versus LASL1050m data which are the most correlated and exhibit the most consistent trends.

4.2 Considering inner length scale effects

To obtain representative l_o from eddy covariance fluxes (Eq. 5), 10 min time averages were used for the following analysis. Missing eddy covariance data and this data aggregation contribute to a decrease in sample size to $N \approx 1000$ samples per transect. XLAS and LASL1050m were used to quantitatively compare C74 and OH82 with and without the consideration of inner length scale effects.

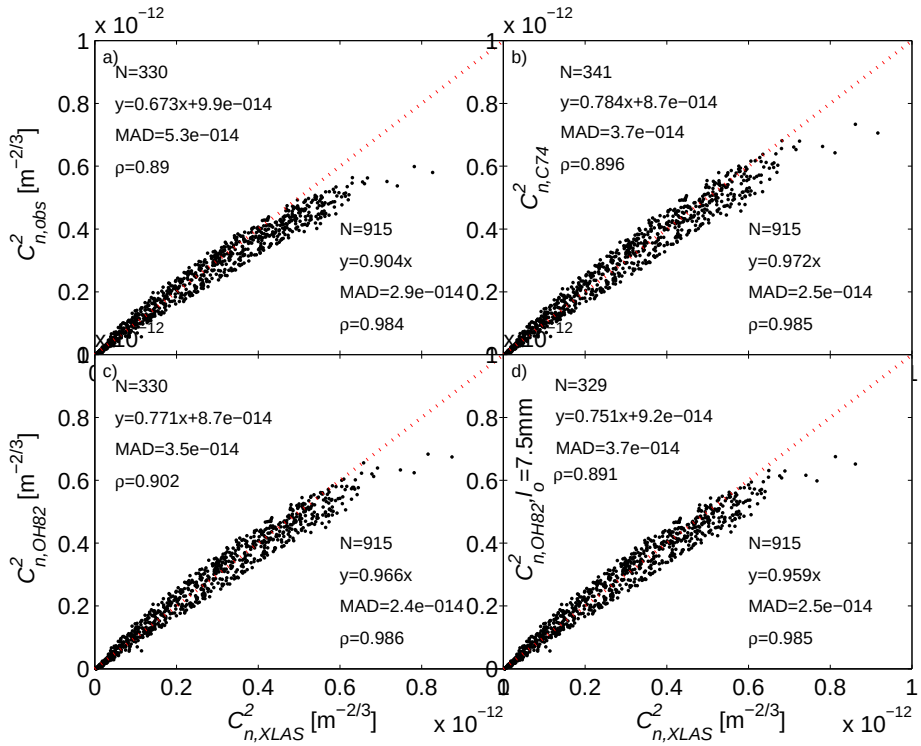

Fig. 7 Scatter plots of (a) calibrated observed C_n^2 and saturation corrected $C_{n,\mathrm{ref}}^2$ following (b) C74, (c) OH82, and (d) OH82 with a constant l_o equal to the average observed in the study. The text on the bottom right in each subplot window shows number of samples, linear regression forced through the origin, mean absolute deviation, and correlation coefficient ρ for the entire dataset. The insert on the top left applies only to the saturated data with $C_n^2 > 3.3 \times 10^{-13}$ m$^{-2/3}$.

Figure 7 shows the C_n^2 measured from LASL1050m against the XLAS, before and after applying the corrections to both scintillometers. The saturation corrections improve the agreement as the regression slopes become closer to 1, the MAD decreases, and ρ increases. For high C_n^2 the actual saturation is larger than the OH82 correction (Fig. 7c,d), consistent with observations by Kohsiek et al. (2006, their Fig. 4). C74 results in a slightly better agreement (Fig. 7b), but the correction is still too small.

If the correction for inner scale effects was accurate, then it should decrease the scatter in the data and increase ρ. In other words, for a given C_n^2 more saturation would be expected to occur for a small l_o than a large l_o. In theory, the OH82 correction then causes a larger correction for the small l_o (Fig. 5), reducing the scatter in Fig. 7c. However, Fig. 7c,d show that the visual spread is the same in the original data, and the OH82 corrected data with and without variable l_o. Although the correlation coefficients for the saturated data increase from 0.891 for $l_o = 7.5$ mm to 0.902 for variable l_o, this small improvement indicates no significant added value of the OH82 inner length scale correction.

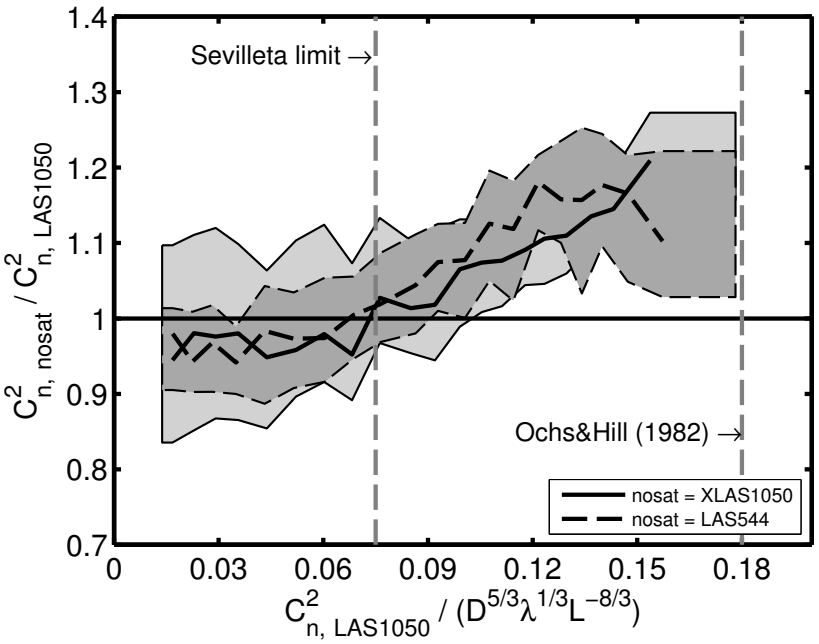

Fig. 8 Ratio of C_n^2 for the less saturated scintillometers (XLAS and LASL544m) divided by C_n^2 from the saturated scintillometer (LASL1050m). The line is smoothed by dividing the variable on the x-axis into 20 bins and taking the median of the x and y values in each bin. The corresponding surfaces of each line mark the inter-quartile range. A departure from 1 indicates saturation. C_n^2 is normalized by $D^{5/3}\lambda^{1/3}L^{-8/3}$ based on Eq. 4 with $B = 3/5$. Then $A = (2\pi)^{-7/10}(0.124E)^{-3/5} = 4.57$, where E is the location on the x-axis where the onset of saturation occurs. The dashed vertical lines show the saturation limit proposed by OH82 and the observed saturation limit, defined as where the smoothed lines become larger than 1.

4.3 Onset of saturation

Comparing the most saturation prone set-up (LASL1050m) with the little to none saturation prone set-ups (XLAS and LASL544m) is an experimental check of the theoretically derived saturation limits (Eq. 4) in Fig. 8. For the LASL1050m Eq. 4 with the factors of OH82 gives a saturation limit of $C_n^2 = 6.22 \times 10^{-13}$ m$^{-2/3}$. In our experiment (Fig. 8) we observed onset of saturation with $C_n^2 = 2.55 \times 10^{-13}$ m$^{-2/3}$ or $C_n^2 > 0.074 D^{5/3}\lambda^{1/3}L^{-8/3}$. The resulting $A = 4.57$ and $B = 3/5$ are in between the values predict by OH82 and Frehlich and Ochs (1990) and correspond to the expression of Moene et al. (2004) with a "safety factor" of 2.1 (Eq. 4).

5 Discussion and conclusions

An experiment, specifically designed to study saturation, was conducted with four scintillometer transects of different lengths and aperture sizes in an arid grassland. Signal saturation was observed in the study and different correction methods were tested. The experimental results show that saturation already occurs at $C_n^2 \approx 0.074 D^{5/3}\lambda^{1/3}L^{-8/3}$ which is less than half the theoretically derived saturation limit by OH82 (Eq. 4).

The saturation correction proposed by C74 provides a simple framework for operational application, since the correction only depends on C_n^2 and transect geometry. Our results show that C74 provides reasonably accurate saturation corrections when two LASs with different aperture size (XLAS with $D = 0.32$ m and LAS with $D = 0.15$ m) are compared over the same pathlength ($L = 1050$ m). The saturation correction proposed by OH82 requires an independent estimate of the inner length scale. While the OH82 correction also results in significant improvements in C_n^2, the correction factors are too small in large saturation regimes. Moreover, the addition of another variable (the inner length scale) does not significantly reduce the scatter in the saturation corrected C_n^2. Against the predictions from both theories, a second LAS ($D = 0.15$ m, $L = 544$ m) saturated more than the XLAS.

For all practical applications with large aperture scintillometers we recommend using the C74 correction method. At a transect length of 1 km, a height of 2.5 m, and aperture ≈ 0.15 m the correction factor exceeds 5% already at $C_n^2 = 2 \times 10^{-12}$ m$^{-2/3}$, which will affect many practical applications of scintillometry, except for those over irrigated fields with small Bowen ratios. Using a numerical look-up table, Scintec's BLSRun data processing software applies the C74 saturation correction operationally. Thus users can apply the correction simply by choosing the respective option in the software. Users of scintillometers from other manufacturers need to derive the coefficients in Table 2 for their respective aperture size, path length, and transect height. A Mathcad program to derive these parameters is available from the authors upon request.

Acknowledgements We acknowledge: funding from USGS-NIWR award number 06HQGR0187 and NMSU-WRRI contract Q01112, UC San Diego startup funding; Sevilleta National Wildlife Refuge staff for assistance with the experiment; Emily Engle and Roger Rentaria for assistance in the field; insightful comments by Henk de Bruin and an anonymous reviewer; instrumentation and access to facilities by Jan Hendrickx, New Mexico Tech.

References

1. Andreas E (1990) Selected papers on turbulence in a refractive medium. *SPIE - The International Society for Optical Engineering, Bellingham.*, **25**, 693pp.
2. Churnside J. (1990): A spectrum of refractive turbulence in the turbulent atmosphere. *Journal of Modern Optics*, **37(1)**, 13–16.
3. Clifford S, Ochs G, Lawrence R (1974): Saturation of optical scintillation by strong turbulence. *J. Opt. Soc. Amer.*, **64**, 148–154.
4. Ezzahar J, Chehbouni A, Hoedjes J, Er-Raki S, Boulet G, Bonnefond JM, de Bruin HAR (2007) The use of the scintillation technique for monitoring seasonal water consumption of olive orchards in a semi-arid region. *Agr. Water Management*, **89**, 173–184.
5. Frenzen P, Vogel CA (1992) The turbulent kinetic energy budget in the atmospheric surface layer: A review and an experimental reexamination in the field. *Boundary-Layer Meteorol.*, **60(1-2)**, 49–76.
6. Frehlich RG, Ochs GR (1990) Effects of Saturation on the Optical Scintillometer. *Appl. Optics.*, **29**, 548–553.
7. Frehlich RG (1992) Laser Scintillation Measurement of the Temperature Spectrum in the Atmospheric Surface Layer. *J. Atmos. Sci.*, **49**, 1494–1509.
8. Hafeez M, Andreini M, Liebe J, Friesen J, Marx A, Giesen N (2006): Hydrological parameterization through remote sensing in Volta basin, West Africa. *Intl. J. River Basin Management*, **4**, 1–8.
9. Hartogensis O (2006) Exploring scintillometry in the stable atmospheric surface layer. Ph.D. thesis, Wageningen University, Wageningen, The Netherlands, 240pp.

10. Hartogensis O, de Bruin HAR (2005) Monin-Obukhov similarity functions of the structure parameter of temperature and turbulent kinetic energy dissipation rate in the stable boundary layer. *Boundary-Layer Meteorol.*, **116(2)**, 253–276.
11. Hartogensis O, Kesteren BV, Evans J, Bradford J, Moene A, Holtslag A (2008) Sensible and latent heat fluxes with an optical and millimeter wave scintillometer system at the Chilbolton test range. *Proceedings 8th Annual Meeting of the European Meteorological Society (EMS), Amsterdam, the Netherlands*.
12. Hartogensis O, Watts C, Rodriguez JC, de Bruin HAR (2003) Derivation of an effective height for scintillometers: La Poza experiment in northwest Mexico. *J. Hydrometeorol.*, **4**, 915–928.
13. Hemakumara H, Chandrapala L, Moene A (2003): Evapotranspiration fluxes over mixed vegetation areas measured from a large aperture scintillometer. *Agric. Water Management*, **58**, 109–122.
14. Hendrickx J, Kleissl J, Gomez-Velez J, Hong SH, Fabrega-Duque J, Vega D, Moreno-Ramirez H, Ogden F (2007): Scintillometer networks for calibration and validation of energy balance and soil moisture remote sensing algorithms. *Proc. International Society for Optical Engineering*, **6565**, 65650W.
15. Hill RJ, Ochs G (1978) Fine calibration of large-aperture optical scintillometers and an optical estimate of inner scale of turbulence. *Applied Optics*, **17(22)**, 3608–3612.
16. Hill RJ, Ochs G, Wilson J (1992) Measuring surface-layer fluxes of heat and momentum using optical scintillation. *Boundary-Layer Meteorol.*, **58**, 391–408.
17. Hill RJ (1981) Saturation resistance and inner-scale resistance of a large-aperture scintillometer: A case study. *Appl. Optics*, **20**, 3822–3824.
18. Hill RJ, Clifford S (1981): Theory of saturation of optical scintillation by strong turbulence for arbitrary refractive-index spectra. *J. Opt. Soc. Amer.*, **71**, 675–686.
19. Hill RJ (1997), Algorithms for obtaining atmospheric surface-Layer fluxes from scintillation measurements, *J. Atmos. Oceanic Tech.*, **14**, 456–467.
20. Kleissl J, Gomez J, Hendrickx J, Hartogensis O, de Bruin HAR (2008b) The Sevilleta scintillometer saturation field experiment. *8th Annual Meeting of the European Meteorological Society*, 7th ECAC, session AW6.
21. Kleissl J, Gomez J, Hong SH, Hendrickx J, Rahn T, Defoor W (2008a) Large aperture scintillometer intercomparison study. *Boundary-Layer Meteorol.*, **128**, 133–150.
22. Kleissl J, Hong SH, Hendrickx J (2009)a: New Mexico scintillometer network: Supporting remote sensing and hydrologic and meteorological models. *Bulletin Am. Meteorol. Soc.*, **90(2)**, 207–218.
23. Kleissl J, Watts C, Rodriguez J, Naif S, Vivoni E (2009)b: Scintillometer intercomparison study - continued. *Boundary-Layer Meteorol.*, **130(3)**, 437–443.
24. Kohsiek W, Meijninger W, de Bruin HAR, Beyrich F (2006) Saturation of the large aperture scintillometer. *Boundary-Layer Meteorol.*, **121**, 111–126.
25. Martano P (1999) Estimation of surface roughness length and displacement height from single-level sonic anemometer data. *J. Applied Meteorol.*, **39(5)**, 708–715.
26. Meijninger W, Hartogensis OK, Kohsiek W, Hoedjes J, Zuurbier R, de Bruin HAR (2002): Determination of area averaged sensible heat fluxes with a large aperture scintillometer over a heterogeneous surface - Flevoland field experiment. *Boundary-Layer Meteorol.*, **105**, 63–83.
27. Moene A, Meijninger W, Hartogensis OK, Kohsiek W, de Bruin HAR (2004) A review of the relationships describing the signal of a Large Aperture Scintillometer. *Internal Report 2004/2, Meteorology and Air Quality Group, Wageningen University, Wageningen, the Netherlands*, 40 pp.
28. Moene A, Meijninger W, Hartogensis OK, Heusinkveld B, de Bruin HAR (2005) The effect of finite accuracy in the manufacturing of large aperture scintillometers. *Internal Report 2005/1, Meteorology and Air Quality Group, Wageningen University, Wageningen, the Netherlands*, 99 pp.
29. Moore C (1986) Frequency response corrections for eddy correlation systems. *Boundary-Layer Meteorol.*, **37(1-2)**, 17–35.
30. Ochs GR, Hill RJ (1982) A study of factors influencing the calibration of optical C_n^2 meters. *NOAA Technical Memorandum ERL WPL-106. Available from: National Technical Information Service, 5285 Port Royal Road, Springfield, VA 22161, U.S.A.*.
31. Schotanus P, Nieuwstadt F, de Bruin HAR (1983) Temperature measurement with a sonic anemometer and its application to heat and moisture fluxes. *Boundary-Layer Meteorol.*, **26(1)**, 81–93.

32. Thiermann V (1996) Surface Layer Scintillometer SLS20/SLS40, User's Manual, Scintec AG, Tubingen, Germany, 74 pp.
33. Wang T, Ochs G, Clifford S (1978) A saturation-resistant optical scintillometer to measure C_n^2. *J. Opt. Soc. Amer.*, **68**, 334–338.
34. Wilczak J, Oncley S, Stage S (2001) Sonic anemometer tilt correction algorithms. *Boundary-Layer Meteorol.*, **99**, 127–150.